

Classification of Amyloid PET Images using novel features for Early Diagnosis of Alzheimer's disease and MCI conversion

¹YuYan ²Ed Somer ¹Vicente Grau

1 University of Oxford, Department of Engineering Science, UK

2 GE Healthcare, Amersham, UK

Research funded by The China Scholarship Council (CSC) and EPSRC and MRC and GE Healthcare

ABSTRACT

New positron emission tomography (PET) tracers could have a substantial impact on early diagnosis of Alzheimer's disease (AD), particularly if they are accompanied by optimised image analysis and machine learning methods. Fractal dimension (FD) analysis, a measure of shape complexity, has been proven useful in MR imaging but its application to fluorine-18 amyloid PET has not yet been demonstrated. Shannon entropy (SE) has also been proposed as a measure of image complexity in DTI imaging, but it is not yet widely used in radiology.

In this study, one volumetric FD method and one volumetric SE method were applied to ^{18}F -flutemetamol and ^{18}F -florbetapir 3D amyloid images from 65 and 281 subjects respectively, including Healthy Volunteers (HV), and patients with probable Alzheimer's Disease (pAD) or Mild Cognitive Impairment (MCI).

The group average fractal dimension of white matter surface and Shannon entropy of white matter volume for HV subjects were higher than for pAD subjects. Both FD and SE are effective in the identification of MCI patients who progress to pAD during the two-year follow-up (ground truth).

Finally, we developed a support vector machine (SVM) multi-modal classification framework using both PET and MRI features, which showed higher accuracy compared to traditional SUVr or using PET alone.

The classification accuracy for flutemetamol and florbetapir is 88.9% and 83.3% respectively for MCI progression, which is competitive with existing literature.

The results presented in this study demonstrate the potential of FD and SE methods for the analysis of brain PET scans in early AD diagnosis and in the prediction of MCI-AD conversion.

Key Words - PET, amyloid imaging, Alzheimer's disease, classification, fractal dimension, Shannon entropy, SVM

INTRODUCTION

Alzheimer's disease (AD) is the most common type of dementia. The brain changes of AD may begin 20 or more years before symptoms appear [1].

The first PET tracer used to image β -amyloid plaques was ^{11}C -Pittsburgh-Compound-B (PiB) [2]. Due to the limited availability of ^{11}C -PiB with its short half-life, ^{18}F -labelled alternatives have been developed, which allow off-site production and regional distribution. ^{18}F -flutemetamol, ^{18}F -florbetapir and ^{18}F -florbetaben have recently been approved by the US Food and Drug Administration (FDA) for clinical use. Abnormal uptake in grey matter causes a disruption of the characteristic white matter pattern caused by non-specific white matter binding. [3] These scans are generally interpreted visually.

A separate group from healthy volunteers (HV) and patients with probable Alzheimer's disease (pAD), mild cognitive impairment (MCI) is an intermediate cognitive state between normal aging and dementia. Subjects with MCI, especially MCI involving memory problems, are more likely to develop AD and other dementias [4]. According to this progression, MCI subjects can subsequently be classified as progressive MCI (pMCI) or stable MCI (sMCI) [5].

In recent years, the focus for image analysis has gradually evolved from classification between healthy control and disease patients to classification between pMCI and sMCI. Most of the earlier studies for MCI conversion were based on a single modality. Min et al. [6] developed a joint learning of optimum representation of features from multiple atlases using maximum margin approach. The method was applied to MRI images with sensitivity and specificity of 76.4% and 70.8% respectively. Another recent single-modality study [7] applied a novel relationship-induced multi-template learning method for automatic diagnosis of AD and MCI on MRI data. The achieved sensitivity and specificity were 87.9% and 75.5%

respectively.

More recent studies have explored classification based on multi-modality data. Cheng et al. [8] integrated a kernel-based maximum mean discrepancy criterion and a manifold regularization function into a combined learning algorithm for both feature selection and classification. Three modalities were used here: MRI, FDG-PET and CSF. The sensitivity and specificity achieved were 85.3% and 73.3% respectively. Chen et al. proposed an embedded novel statistical learning approach in a multi-kernel framework for longitudinal, multimodal data. They achieved 91% accuracy for pMCI vs sMCI classification [9]. These results demonstrate promising classification performance compared with several state-of-the-art methods for single modality based MCI conversion classification.

A recent review [10] highlights that the use of novel features from amyloid PET to classify MCI to AD progression has not been widely explored. In this work, we apply Fractal Dimension (FD) analysis, a measure of uptake pattern complexity, to amyloid PET scans. As the disease progresses and plaques build, the characteristic white matter pattern seen in normal subjects becomes increasingly obscured by the presence of uptake in grey matter. This leads to a decrease of the complexity of the isocontours of the PET images. We hypothesise that this decrease in complexity can be detected using fractal dimension analysis. This is the approach we demonstrate in the present work.

Shannon entropy (SE) is an alternative complexity measure to FD that quantifies the information content of the data [11]. While SE has been used in electrocardiographic (ECG) analysis [12], it is not well-known or widely used in radiology. Recently, SE [13] was investigated as a diagnostic tool in patients with mild traumatic brain injury (TBI) in diffusion tensor imaging, to differentiate between those with and without posttraumatic migraines (PTMs). The results show that white-matter damage from a mild traumatic injury

may cause some decrease of image complexity that results in lower SE. To our knowledge, SE has not been used in the study of PET images up to date.

In addition, many previous works have shown that MRI offers information complementary to PET-derived features such as morphological features [14]. Daoqiang et.al [15] proposed a multi-modal classification framework for MCI conversion prediction, and they found that the multimodality method shows considerably better performance, compared to the case of using biomarkers from an individual modality. More recently, Juergen et.al [16] developed a meta-analysis based SVM classification model using FDG-PET and MRI, which outperformed single modality as well.

After the calculation of specific features, a range of classifiers have been used in related work. Among these, Support Vector Machines (SVMs) have been used for prediction of conversion from MCI to AD with relatively high accuracy. Liu et al. [17] proposed an inherent structure-based multi-view learning method using multiple templates for AD/MCI classification, with an SVM classifier used to draw the final decision. They achieved a classification accuracy of 80.9%. Costafreda et al. [18] also combined the shape and volumetric features of the hippocampus for SVM-based AD conversion prediction. Their model correctly predicted MCI conversion to AD with an accuracy of 80%.

In this study, we propose, for the first time, the application of fractal dimension (FD) and Shannon entropy (SE) to the analysis of complexity of amyloid PET images. We augment FD and SE by combining these with standard uptake value ratio (SUVr) and MRI features generated from the FreeSurfer pipeline, feeding these into an SVM classifier to identify Alzheimer's disease and predict MCI progression.

MATERIALS AND METHODS

Data

Two sets of data were used in the preparation of this article. The first was obtained from GE Healthcare, and included ^{18}F -flutemetamol PET and MRI scans for 65 subjects (24 HV, 23 pAD and 18 MCI, divided into 9 sMCI and 9. pMCI). The subjects were recruited into the study from multiple clinical study sites. The inclusion criteria of the different subject groups are described on ClinicalTrials.gov (Identifier: NCT00785759). To diagnose pAD and assess MCI progression, there was an initial assessment at study enrolment (baseline) with a subsequent assessment 2 years later. The clinical assessment included physical symptoms, blood tests and a variety of mental tests. The flutemetamol image dimensions are $128 \times 128 \times 81$ with a voxel size of $2.13\text{mm} \times 2.13\text{mm} \times 2\text{mm}$. Screening MRI scanning was performed for each subject prior to PET scanning. MRI images were acquired using 3D T1-weighted sequence (MPRAGE) with the whole brain in the field of view for all images.

On the day of PET imaging, each subject received an intravenous dose of ^{18}F -flutemetamol as a bolus injection. The target activity of a single administration of ^{18}F -flutemetamol injection was 185 MBq. Three scanning sites were used: Liege and Leuven in Belgium and Rigshospitalet in Denmark. The images were acquired 30 minutes after the injection and were analysed by five expert clinicians who were blinded to the clinical diagnosis and all other clinical findings; the consensus of this blinded image evaluation (BIE) was available for our study. The gold standard was assessed at two years follow up for AD conversion by measuring ranges of regional cerebral to cerebellum tracer uptake ratios.

For ^{18}F -florbetapir data, 36 pAD, 82 HV, 29 pMCI and 134 sMCI ^{18}F -florbetapir images with corresponding MRI were obtained from the ADNI database [19]. The PET and MRI volumes for each subject selected for

this study were acquired no more than 12 months apart. All the subjects have at least two years follow up, which we use as gold standard for AD conversion (sMCI if the status of MCI remains throughout 2 years follow up and pMCI if MCI label changes to AD in the follow up).

Pre-processing

All the florbetapir images had been already pre-processed by ADNI: MRI and PET scans from each subject were co-registered, and the image from their baseline PET scan was then reoriented into a standard $160 \times 160 \times 96$ voxel image grid, comprising 1.5 mm cubic voxels. This image grid was oriented such that the anterior-posterior axis of the subject is parallel to the AC-PC line. The corresponding MRI images have dimensions $256 \times 256 \times 196$ with a voxel size of $1\text{mm} \times 1\text{mm} \times 1.2\text{mm}$.

Flutemetamol images were obtained in their original state from the GE study and thus needed to be pre-processed as follows. As a first step, image intensities were rescaled to [0 255], and then the segmentation of the white matter in the PET images was performed using a hysteresis thresholding method [20]. This segmentation method performs a dual thresholding operation on a grayscale image using two threshold values. We followed this by an erosion operation. The white matter masks calculated in this way were used in two ways: a) to binarise the original images for the calculation of FD; and b) to remove all image values outside of the mask (by making them zero), while keeping the original image intensities inside the mask: the images obtained in this way were used for the calculation of SE. Examples of original T1 MRI, flutemetamol PET images, with their corresponding segmented label maps are shown in Figure 1.

Secondly, the PET volumes were rigidly registered to their corresponding MR volumes using FSL's FLIRT software [21]. The MR volumes were then affinely registered to Montreal Neurological Institute (MNI) space using Statistical Parametric Mapping, version 12 (SPM12), [22] and the resulting transformations

were applied to the PET volumes.

Calculation of Fractal Dimension using the Box Counting Method

In order to calculate features based on fractals, here we applied a box counting (dilation) method to compute the fractal dimension from binary images.

The original box counting method consists of partitioning the structure space with a three dimensional fixed grid of boxes of equal size r . The box sizes correspond to powers of 2, ranging in our case from 0 to 4 [23].

In fractal structures, the number N_r of nonempty boxes of size r needed to cover the fractal structure depends on r according to the following equation:

$$N_r \sim r^{-FD} \quad (1)$$

The box counting algorithm hence counts the number N_r for different values of r and plots the log of the value N_r versus the log of the box size r . The value of FD is then estimated from the slope of least squares best fitting curve:

$$FD = \lim_{r \rightarrow 0} \frac{\log(N_r)}{\log(1/r)} \quad (2)$$

In practical applications, when studying objects that are not pure fractals, the limit $\lim_{r \rightarrow 0}$ is not attainable.

Instead, N_r is measured for a limited range of r values corresponding to intermediate resolutions of the object under study. Here a dilation algorithm was implemented using a 3D convolution. The voxel dilation method replaces each voxel in the white matter surface by a cube with size r . This provides a more precise version than the original box counting algorithm. Subsequently, fractal dimension is then estimated by approximating Eq. 2.

Shannon entropy

Shannon introduced another complexity measure [11], which weighs the information per outcome by the probability of that outcome occurring. Given events e_1, \dots, e_m occurring with probabilities p_1, \dots, p_m , the Shannon entropy H is defined as

$$H = \sum_i p_i \log \frac{1}{p_i} = -\sum_i p_i \log p_i \quad (3)$$

In the medical image processing field, entropy has been used as a statistical metric to characterize texture distribution [24]. To calculate the Shannon entropy of the white matter volume, the probability of occurrence for each intensity value in the white matter volume is needed. We estimated the probability distribution values p_i by normalizing the histogram of voxel intensities in the white matter volume.

SVM Classification

In this study, a two class SVM classifier is used to classify different groups of subjects. In its simplest form, the SVM method constructs a hyperplane that maximizes the margin, defined as the distance between the closest points on either side of the calculated boundary.

Here we apply an SVM with a non-linear kernel using radial basis functions, using the implementation in the SVM package LIBSVM, running under Matlab version 8.6 [25].

Experiments

65 flutemetamol images (23 pAD and 24 HV, 9 pMCI and 9 sMCI) and 281 florbetapir images (36 pAD and 82 HV, 134 sMCI and 29 pMCI) were used for this study.

Firstly, we applied the hysteresis segmentation to the unprocessed PET images. The threshold values t_1 and t_2 (between 0 and 1) were set empirically to 0.3 and 0.5 respectively. Three-dimensional 6-connected neighborhoods were searched from each object voxel. Binary erosion was applied to the segmented binary image to extract the surface, using a cube structuring element with size 3. After this step,

box counting and Shannon entropy were applied to the white matter binary image (surface) and white matter original intensity image (volume) respectively.

Secondly, SUVr in each of four lobes (frontal lobe, parietal lobe, occipital lobe, and temporal lobe) were calculated from the co-registered PET images using the MNI atlas. The reference region for SUVr computation was the cerebellum. The resulting SUVr values from all lobes were fed to a SVM classifier to make a decision for pAD and HV, pMCI and sMCI.

Finally, FD, SE and MRI features (hippocampus volume, lateral ventricle volume and cortical thickness generated from standard FreeSurfer pipeline) were then combined with SUVr [26]. Due to the limited number of flutemetamol images, a leave one out cross validation was performed for these data sets: one subject was taken as a test set and the remaining as training set, and this process was repeated 65 times. For each of the leave-one-out experiments, a 3-fold cross validation was used on the 64 subjects in the training set to find the optimal parameters C and γ for the nonlinear support vector machine with a Gaussian radial basis function kernel. The resulting classifier was then used on the single testing set.

The florbetapir set was larger ($n=281$) and thus we chose to perform 10-fold cross validation on it. 253 subjects were taken as training set and the remaining 28 subjects as test set. 3-fold cross validation was applied within the training set to find the optimal parameters as before.

In this study, PET and MRI features were computed from all 65 flutemetamol images and 281 florbetapir images. Both PET and MRI features were combined with SUVr to predict HV and pAD, pMCI and sMCI.

The classification results were compared with BIE and most recent results from literature. In all cases, the gold standard for pAD classification was clinical diagnosis, and for MCI progression was two-year follow-up.

RESULTS

The flutemetamol classification results between pAD and HV were compared with the BIE majority read, which achieved 88% sensitivity and 96% specificity. In addition, the MCI group at baseline were analyzed using the proposed methods and compared with progression status in the follow-up evaluation. In this case, BIE achieved 78% sensitivity and 78% specificity.

Both FD and SE performed well for the classification of flutemetamol images as disease positive or disease negative. The sensitivity and specificity of FD were 85.7% and 89% respectively, while the sensitivity and specificity of the SE method were 87% and 92.6%. The performance of the classification of MCI subjects as progressed or stable was also evaluated. For FD, sensitivity and specificity were 78% and 89% respectively. SE reached sensitivity 89% and specificity 78%, which compared favorably with the BIE results. Figure 2 shows the variation in FD and SE between the three groups, as well as the ROCs for MCI conversion classification.

For PET features comparison, the SVM classification accuracy for both flutemetamol and florbetapir are shown in Table 1. The top part of the Table presents results achieved with PET images only. As can be seen, both FD and SE alone outperformed the traditional SUV_r method in pAD/HV and pMCI/sMCI classifications. Several feature combinations produced the same highest accuracy (91.5%) for pAD vs HV classification. The highest accuracy for pMCI vs sMCI classification was obtained by using flutemetamol PET features, which reached 83.3% with the combination of SUV_r, FD and SE. The accuracy decreased slightly to 80.4% when using 281 florbetapir images with the same feature combination.

In addition, the results of combining PET features and corresponding MRI features from FreeSurfer are shown in the bottom part of Table 1. As expected, the highest accuracy was achieved when combining all

PET and MRI features. The highest classification accuracy for pAD vs HV was 93.6% and 93.2% for the flutemetamol and florbetapir groups, respectively. The highest classification accuracy between pMCI and sMCI was 88.9% and 82.8% for the flutemetamol and florbetapir groups, respectively. We compared these results with recent state of the art in image-based (i.e. excluding non-imaging tests) classification [27 28 29 30]. As shown in Table 2, our method outperformed recent results from previously published studies in the prediction of MCI conversion, and obtained competitive accuracy in the classification of pAD vs HV, when comparing versions using PET information only as well as those combining PET and MRI features.

DISCUSSION AND CONCLUSION

In this paper two complexity measurements were proposed for amyloid status classification, namely fractal dimension and Shannon entropy methods. Both FD and SE outperformed the traditional SUVr, both for the identification of pAD vs HV subjects and for identification of subjects likely to convert from MCI to pAD. Individual application of FD and SE improved on the individual application of SUVr. When FD and SE were combined, an additional modest improvement was observed, suggesting some complementarity of the information from each. The best results for PET-only classification were obtained when SUVr, FD and SE were combined together. As an additional advantage, in our framework FD and SE are calculated directly on the images on a straightforward manner, while SUVr was parcellated into four lobes with the help of an external atlas.

The SVM classification results indicated the ability of using ^{18}F PET features alone, and also pointed out the importance of introducing MR features, which resulted in a marked increase of the accuracy when compared to PET-only calculation in both the flutemetamol and florbetapir groups. However, these clearly introduced some information complementary from that in the PET as shown in the fact that the combination

between MRI, FD, SE and SUVr (calculated on a lobar basis) resulted in the best classification overall.

Results were competitive with existing literature, particularly on the prediction of MCI conversion.

ACKNOWLEDGEMENTS

We would like to acknowledge support from the China Scholarship Council (CSC) and The Engineering and Physical Sciences Research Council (EPSRC) and Medical Research Council (MRC) [grant number EP/L016052/1] and GE healthcare

REFERENCE

- [1] Braak, H.; Braak, E. (1991). "Neuropathological staging of Alzheimer-related changes". *Acta Neuropathologica*. 82 (4): 239–59. doi:10.1007/BF00308809. PMID 1759558.
- [2] Klunk, W.E., Engler, H., Nordberg, A., Wang, Y., Blomqvist, G., Holt, D.P., et.al. 2004. Imaging brain amyloid in Alzheimer's disease with Pittsburgh Compound - B. *Annals of neurology*, 55(3), pp.306-319.
- [3] Knesaurek, Karin, et al. "Comparison of SUVr calculations in amyloid PET brain imaging." *Journal of Nuclear Medicine* 55.supplement 1 (2014): 1873-1873.
- [4] Villemagne, V.L., Burnham, S., Bourgeat, P., Brown, B., Ellis, K.A., Salvado, O., et.al. 2013. Amyloid β deposition, neurodegeneration, and cognitive decline in sporadic Alzheimer's disease: a prospective cohort study. *The Lancet Neurology*, 12(4), pp.357-367.
- [5] Thurfjell, L., Lötjönen, J., Lundqvist, R., Koikkalainen, J., Soininen, H., Waldemar, G et.al. 2012. Combination of biomarkers: PET [18F] flutemetamol imaging and structural MRI in dementia and mild cognitive impairment. *Neurodegenerative Diseases*, 10(1-4), pp.246-249.
- [6] Min, R., Cheng, J., Price, T., Wu, G. and Shen, D., 2014, September. Maximum-margin based representation learning from multiple atlases for Alzheimer's disease classification. In *International Conference on Medical Image Computing and Computer-Assisted Intervention* (pp. 212-219). Springer, Cham.
- [7] Liu, M., Zhang, D. and Shen, D., 2016. Relationship induced multi-template learning for diagnosis of

Alzheimer's disease and mild cognitive impairment. *IEEE transactions on medical imaging*, 35(6), pp.1463-1474.

[8] Cheng, B., Liu, M., Suk, H.I., Shen, D., Zhang, D. and Alzheimer's Disease Neuroimaging Initiative, 2015. Multimodal manifold-regularized transfer learning for MCI conversion prediction. *Brain imaging and behavior*, 9(4), pp.913-926.

[9] Chen T, Zeng D, Wang Y. Multiple kernel learning with random effects for predicting longitudinal outcomes and data integration. *Biometrics* 2015; 71:918–28.

[10] Weiner, M.W., Veitch, D.P., Aisen, P.S., Beckett, L.A., Cairns, N.J., Green, R.C., et.al. 2017. Recent publications from the Alzheimer's Disease Neuroimaging Initiative: Reviewing progress toward improved AD clinical trials. *Alzheimer's & dementia: the journal of the Alzheimer's Association*, 13(4), pp.e1-e85.

[11] Shannon CE The mathematical theory of communication. 1963. *MD Comput* 14: 306–317.

[12] Basu, Sautami, and Yusuf U. Khan. "On the aspect of feature extraction and classification of the ECG signal." 2015 *Communication, Control and Intelligent Systems (CCIS)*. IEEE, 2015.

[13] Delic, J., Alhilali, L.M., Hughes, M.A., Gumus, S. and Fakhran, S., 2016. White matter injuries in mild traumatic brain injury and posttraumatic migraines: diffusion entropy analysis. *Radiology*, 279(3), pp.859-866.

[14] Rathore, S., Habes, M., Iftikhar, M.A., Shacklett, A. and Davatzikos, C., 2017. A review on neuroimaging-based classification studies and associated feature extraction methods for Alzheimer's disease and its prodromal stages. *NeuroImage*, 155, pp.530-548.

[15] Zhang, Daoqiang, et al. "Multimodal classification of Alzheimer's disease and mild cognitive impairment." *Neuroimage* 55.3 (2011): 856-867.

-
- [16] Dukart, Juergen, et al. "Meta-analysis based SVM classification enables accurate detection of Alzheimer's disease across different clinical centers using FDG-PET and MRI." *Psychiatry Research: Neuroimaging* 212.3 (2013): 230-236.
- [17] Liu, M., Zhang, D., Adeli, E. and Shen, D., 2016. Inherent Structure-Based Multiview Learning With Multitemplate Feature Representation for Alzheimer's Disease Diagnosis. *IEEE Transactions on Biomedical Engineering*, 63(7), pp.1473-1482.
- [18] Costafreda, S.G., Dinov, I.D., Tu, Z., Shi, Y., Liu, C.Y., Kloszewska, I., et.al. 2011. Automated hippocampal shape analysis predicts the onset of dementia in mild cognitive impairment. *Neuroimage*, 56(1), pp.212-219.
- [19] Weiner, M.W., Veitch, D.P., Aisen, P.S., Beckett, L.A., Cairns, N.J., Cedarbaum, J., et.al. 2015. 2014 Update of the Alzheimer's Disease Neuroimaging Initiative: a review of papers published since its inception. *Alzheimer's & dementia: the journal of the Alzheimer's Association*, 11(6), pp.e1-e120.
- [20] Xie, L., Sparks, M.A., Li, W., Qi, Y., Liu, C., Coffman, T.M. et.al. 2013. Quantitative susceptibility mapping of kidney inflammation and fibrosis in type 1 angiotensin receptor - deficient mice. *NMR in biomedicine*, 26(12), pp.1853-1863.
- [21] Jenkinson, M., Bannister, P.R., Brady, J.M., Smith, S.M., 2002. Improved optimisation for the robust and accurate linear registration and motion correction of brain images. *NeuroImage* 17 (2), 825–841.
- [22] Penny, William D., et al., eds. *Statistical parametric mapping: the analysis of functional brain images*. Elsevier, 2011.
- [23] Madan, Christopher R., and Elizabeth A. Kensinger. "Cortical complexity as a measure of age-related brain atrophy." *NeuroImage* 134 (2016)

-
- [24] Bhakta, I. and Phadikar, S., 2017. Evaluation of Entropy-Based Segmentation Techniques for Automated Skin Disease Detection. In Proceeding of International Conference on Intelligent Communication, Control and Devices (pp. 335-341). Springer, Singapore.
- [25] C.-C. Chang and C.-J. Lin. LIBSVM : a library for support vector machines. *ACM Transactions on Intelligent Systems and Technology*, 2:27:1--27:27, 2011. pdf, ps.gz, ACM digital lib.
- [26] Fischl, Bruce, and Anders M. Dale. "Measuring the thickness of the human cerebral cortex from magnetic resonance images." *Proceedings of the National Academy of Sciences* 97.20 (2000): 11050-11055.
- [27] Lange C, Suppa P, Frings L, BrennerW, Spies L, Buchert R. Optimization of Statistical Single Subject Analysis of Brain FDG PET for the Prognosis of Mild Cognitive Impairment to Alzheimer's Disease Conversion. *J Alzheimers Dis* 2015;49:945–59.
- [28] Vandenberghe, R., Nelissen, N., Salmon, E., Ivanoiu, A., Hasselbalch, S., Andersen, A., et.al. 2013. Binary classification of 18F-flutemetamol PET using machine learning: comparison with visual reads and structural MRI. *NeuroImage*, 64, pp.517-525.
- [29] Zu, C., Jie, B., Liu, M., Chen, S., Shen, D., Zhang, D. et.al. 2016. Label-aligned multi-task feature learning for multimodal classification of Alzheimer's disease and mild cognitive impairment. *Brain imaging and behavior*, 10(4), pp.1148-1159.
- [30] Cheng B, Liu M, Zhang D, Munsell BC, Shen D. Domain Transfer Learning for MCI Conversion Prediction. *IEEE Trans Biomed Eng* 2015;62: 1805–17.

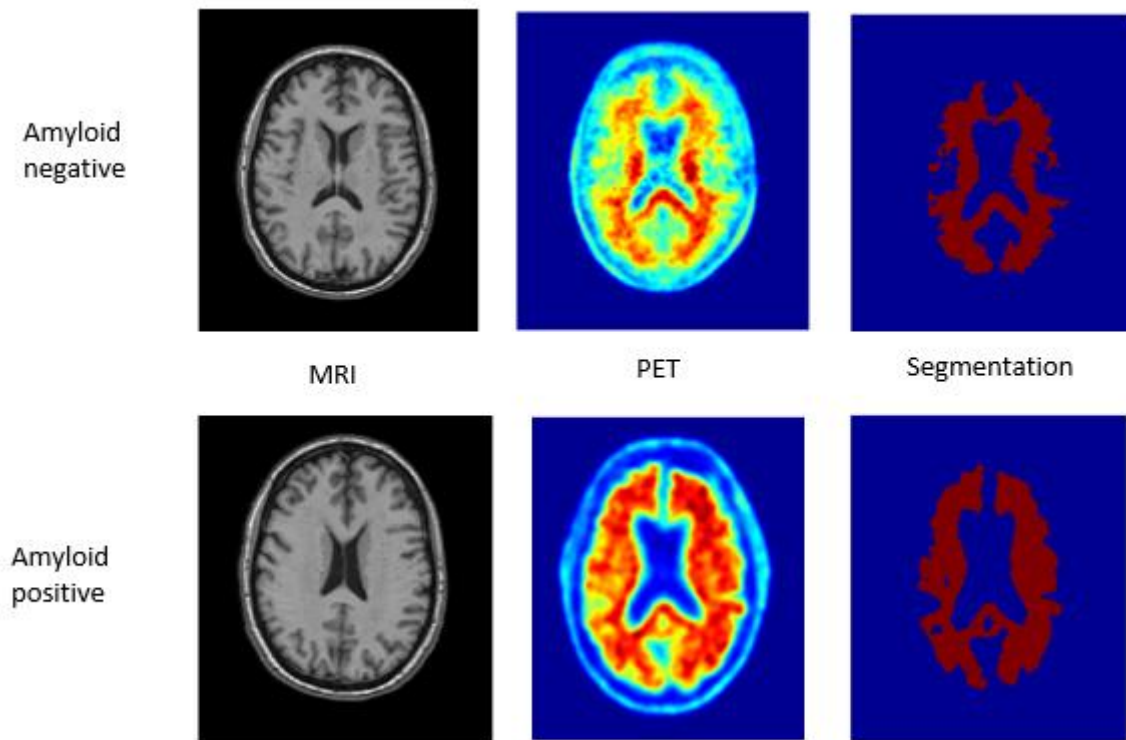


Figure 1: amyloid negative and positive axial slices from left to right: T1 MRI images; flutemetamol PET images; hysteresis segmentation of WM region using hysteresis thresholding.

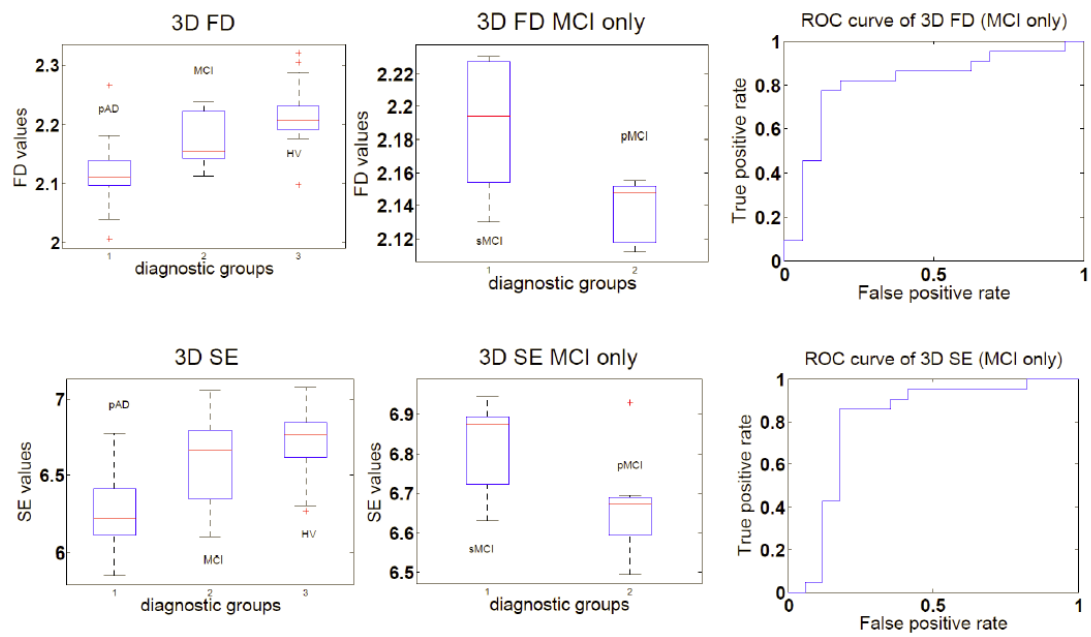


Figure 2: (a) 3D FD box plot for three disease states (b) 3D FD box plot for MCI only (c) ROC for 3D FD (d) 3D SE box plot for three disease states (e) 3D SE box plot for MCI only (f) ROC for 3D SE using 65 flutemetamol images.

	Number of features per subject	pAD and HV accuracy		pMCI and sMCI accuracy	
		Flutemetamol	Florbetapir	Flutemetamol	Florbetapir
FD	1	89.4	86.4	77.8	77.9
SE	1	89.4	87.3	72.2	77.3
FD+SE	2	91.5	90.7	77.8	79.1
SUVr	4	85.1	84.7	66.7	71.8
SUVr+SE	5	89.4	89	77.8	78.5
SUVr+FD	5	91.5	91.5	83.3	79.8
SUVr+FD+SE	6	91.5	91.5	83.3	80.4
<hr/>					
MRI	6	78.7	76.3	66.7	71.8
MRI+SUVr	10	87.2	86.4	72.2	77.3
MRI+FD+SE	8	91.5	90.7	83.3	82.8
MRI+FD+SE +SUVr	12	93.6	93.2	88.9	82.8

Table 1: SVM classification accuracy for 65 flutemetamol and 281 florbetapir images. The top part of the Table presents results obtained using PET-derived features only, while the bottom part includes MRI-derived features too.

Reference	Modalities	Classifier	Number of subjects	Accuracy pAD vs HV	Accuracy pMCI vs sMCI
[27]	FDG-PET	T-sum score	108	N/A	68.5
[28]	Flutemetamol PET	SVM	72	Sensitivity 85.2 Specificity 92	N/A
Proposed method	Flutemetamol PET	SVM	65	91.5	83.3
	Florbetapir PET		281	91.5	80.4
[29]	MRI FDG-PET	SVM	202	95.6	69.8
[30]	MRI FDG-PET CSF	SVM	202	N/A	76.5
Proposed method	MRI Flutemetamol PET	SVM	65	93.6	88.9
	MRI Florbetapir PET		281	93.2	82.8

Table 2: Comparison between our proposed methods and previously published studies